# The Importance of Ion−Neutral Complexes in Gas-Phase Ionic Reactions: Fragmentation of $[CH_3CH_2OCH_2]^+$ as a Prototypical Case

**Andrew J. Chalk and Leo Radom***

*Contribution from the Research School of Chemistry, Australian National University, Canberra, ACT 0200, Australia*

*Received December 9, 1997*

**Abstract:** High level ab initio calculations performed at the G2 level have been used to characterize the potential energy surface for rearrangement and fragmentation of $[CH_3CH_2OCH_2]^+$. Ion−neutral complexes play a crucial role in the lowest-energy decomposition leading to elimination of water. RRKM calculations on the G2 surface are found to give results consistent with the experimentally observed metastable ion elimination products and with the results of various deuterium- and $^{13}C$-labeling experiments. The consequences of producing $[CH_3CH_2OCH_2]^+$ by isomerization from $[CH_3CHOCH_3]^+$ and of producing $[CH_3CH_2CHOH]^+$ by isomerization from $[CH_3C(OH)CH_3]^+$ in relation to the rearrangement/fragmentation behavior are examined and found to be nicely consistent with experimental observations. Experimental thermochemical quantities such as rate-limiting barriers and heats of formation are found generally to be in good agreement with calculated values.

## Introduction

It is more than 40 years since Myerson invoked ion−neutral complexes to explain the loss of identity of labels in the benzyl ions produced from *tert*-butylbenzene.[1] Since that time, ion−neutral complexes have been found to be ubiquitous in gas-phase ionic reactions.[2] Simple electrostatics *demands* that when an ion encounters a neutral species in the gas phase, the energy initially decreases. This means that either the product is formed directly without a barrier or there is the initial involvement of an ion−neutral complex before a barrier is surmounted on the way to the product. A classical example is the $S_N2$ reaction of $X^-$ with $CH_3Y$, for which the gas-phase reaction profile involves a reactant ion−neutral complex $[X\cdots CH_3Y]^-$ leading to a transition structure $[X\cdots CH_3\cdots Y]^-$ and then a product ion−neutral complex $[XCH_3\cdots Y]^-$.[3] In contrast, the text book reaction profile of the $S_N2$ reaction in solution does not involve ion−neutral complexes but proceeds simply from reactants to the transition structure $[X\cdots CH_3\cdots Y]^-$ and then to products. The ion−neutral complexes lose their relevance when complexation with solvent, that is, solvation, is possible.

Ion−neutral complexes have been postulated as intermediates in elaborate mechanisms that attempt to explain the formation of unusual products in gas-phase ionic reactions.[2] For example, the means by which $H_2O$ is lost from $[CH_3CH_2OCH_2]^+$ is not at all obvious. However, its formation has been rationalized in terms of an imaginative mechanism involving the participation of a series of ion−neutral complexes (Scheme 1).[4] It is not straightforward to experimentally verify the involvement of the postulated ion−neutral complexes and to characterize them in detail. In addition, it is not clear which species in mechanistic schemes such as Scheme 1 represent true intermediates on the potential energy surface as opposed, for example, to transition structures. The term "transitional species" has been used to describe some of the less well defined entities.[2a] Although difficult to answer experimentally, such issues *can* be addressed theoretically. Both the ion−neutral complexes and the transition structures of Scheme 1 can be fully characterized, and the reaction path joining the individual species can be followed.

**Scheme 1**

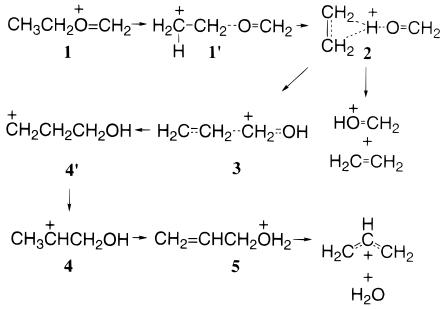


The dissociation of the $[CH_3CH_2OCH_2]^+$ cation represents an attractive prototype for the study of the involvement of ion−neutral complexes in gas-phase chemical reactions. There have been a number of relevant experimental studies on this system. Tsang and Harrison reported the metastable mass spectrum of $[CH_3CH_2OCH_2]^+$ and $[CH_3CHOCH_3]^+$ ions in 1970.[5] After several other studies,[6,7a,8] including an experimental determination of energy barriers,[6] the rearrangement and dissociation mechanism of Scheme 1 was proposed by Bowen and Williams

(1) Rylander, P. N.; Meyerson, S. *J. Am. Chem. Soc.* **1956**, *78*, 5799.
(2) For recent reviews on ion−neutral complexes, see, for example: (a) Bowen, R. D. *Acc. Chem. Res.* **1991**, *24*, 364. (b) Longevialle, P. *Mass Spectrom. Rev.* **1992**, *11*, 157. (c) McAdoo, D. J.; Morton, T. H. *Acc. Chem. Res.* **1993**, *26*, 295.
(3) See, for example: Shaik, S.; Schlegel, H. B.; Wolfe, S. *Theoretical Aspects of Physical Organic Chemistry: The $S_N2$ Mechanism*; Wiley: New York, 1992.
(4) Bowen, R. D.; Williams, D. H. *J. Am. Chem. Soc.* **1978**, *100*, 7454.
(5) Tsang, C. W.; Harrison, A. G. *Org. Mass. Spectrom.* **1970**, *3*, 647.
(6) (a) Yeo, A. N. H.; Williams, D. H. *J. Am. Chem. Soc.* **1971**, *93*, 395. (b) Tsang, C. W.; Harrison, A. G. *Org. Mass Spectrom.* **1973**, *7*, 1377. (c) McLafferty, F. W.; Sakai, I. *Org. Mass Spectrom.* **1973**, *7*, 971.
(7) (a) Hvistendahl, G.; Williams, D. H. *J. Am. Chem. Soc.* **1975**, *97*, 3097. (b) Hvistendahl, G.; Bowen, R. D.; Williams, D. H. *J. Chem. Soc., Chem. Commun.* **1976**, 294.
(8) (a) Williams, D. H.; Bowen, R. D. *J. Am. Chem. Soc.* **1977**, *99*, 3192. (b) Bowen, R. D.; Kalman, J. R.; Williams, D. H. *J. Am. Chem. Soc.* **1977**, *99*, 5481.

S0002-7863(97)04178-4 CCC: $15.00 
Published on Web 08/08/1998

in 1978.[4] Extensive labeling experiments and studies of other $[C_3H_7O]^+$ isomers have been performed[7b,9−12] and alternatives to Scheme 1 have also been proposed.[10] Theoretical work reported on these systems includes calculations of the structures and energies of many of the $[C_3H_7O]^+$ isomers at the MP3/6-31G(d)//HF/3-21G level,[13] while a recent important study[12] has examined in detail the rearrangement and dissociation processes at the MP2/6-31G(d)//HF/6-31G(d) level.

The present study aims to examine the mechanism of Scheme 1 and other related processes using levels of theory higher than those previously applied to the problem. We characterize rigorously the various species encountered on the potential energy surface as equilibrium structures or transition structures and, with the aid of RRKM calculations, compare our results with available experimental information.

## Methods and Results

Standard ab initio molecular orbital calculations[14] were carried out with the GAUSSIAN 94[15] and MOLPRO[16] programs using a slight modification of the G2[17] level of theory. G2 theory was introduced by Pople and co-workers with the aim of predicting thermochemical data to so-called chemical accuracy, roughly 10 kJ mol$^{-1}$. It corresponds effectively to calculations at the QCISD(T)/6-311+G(3df,2p) level on MP2/6-31G(d)-optimized structures together with a zero-point vibrational energy (ZPE) correction calculated at the HF/6-31G(d) level and a so-called higher-level correction (HLC). For the potential surface examined in the present study, we have found some significant differences between the HF/6-31G(d) and MP2/6-31G(d) results and we have therefore used MP2/6-31G(d) frequencies (scaled by 0.9646)[18] in place of HF/6-31G(d) (scaled by 0.8929) in the G2 analysis. This procedure (which requires a modified HLC) has been referred to as G2(ZPE=MP2),[19] but for brevity we simply use the G2 label in the present paper. The MP2 geometry and frequency calculations are performed with all electrons correlated, that is, MP2(full).

Heats of formation at 298 K have been calculated using the atomization method, with temperature corrections applied as described by Nicolaides et al.[20] using scaled (by 1.0084[21]) MP2/6-31G(d) frequencies.

The dependence of the rate constant $k(E)$ of a unimolecular reaction on the internal energy ($E$) of a species can be calculated using RRKM theory,[22] which can be formulated as

$$k(E) = \frac{\sigma N^{\ddagger}(E - E_0)}{h\rho(E)} \quad (1)$$

where $E$ is the internal energy (relative to the reactant), $E_0$ is the energy of the transition structure, $\sigma$ is the reaction path degeneracy, $N^{\ddagger}(E - E_0)$ is the number of states in the transition structure with energy less than or equal to $E$, $\rho(E)$ is the density of states of the reactant, and $h$ is Plank's constant. In the present study, both the sum and density of states were obtained via direct count of the vibrational states using the Beyer−Swinehart algorithm.[22,23] These calculations employed calculated MP2/6-31G(d) frequencies scaled by a factor of 0.9427.[21] Because there is no formal transition structure for direct formaldehyde elimination from $[CH_3CH_2OCH_2]^+$ or ethylene elimination from the ion−neutral complexes, the transition structure frequencies for these dissociations were obtained from the calculated frequencies for the appropriate reactant by removing one frequency corresponding to the reaction coordinate and scaling the lowest five frequencies to give a value for $\Delta S^{\ddagger}$ (600 K) of approximately +15 J K$^{-1}$ mol$^{-1}$.[22b,24]

Calculated G2 total energies are listed in Table S1 of the Supporting Information. Selected geometrical features are displayed in Figure 1, while complete geometries are presented in the form of GAUSSIAN archive files in Table S2. A schematic potential energy profile is displayed in Figure 2. Unless otherwise stated, all relative energies in the text refer to G2 values at 0 K obtained in the above manner, and all geometric information refers to MP2/6-31G(d)-optimized structures.

## Discussion

**Structural and Energetic Features of the Potential Surface.** The most notable geometrical feature for the starting $[CH_3CH_2OCH_2]^+$ cation (**1**) is a C−O bond length (1.522 Å, Figure 1) which is significantly greater than that of typical C−O bonds (e.g., 1.424 Å in $CH_3OH$ at MP2/6-31G(d)). In this sense, the geometry is part of the way toward a $[CH_3CH_2\cdots OCH_2]^+$ structure, that is, it is intermediate between **1** and **1′** of Scheme 1. We do not find a separate minimum corresponding to **1′** although **TS:1→2** resembles the proposed structure of **1′**.

A 1,3-hydrogen migration via **TS:1→2** at 109 kJ mol$^{-1}$ (Figure 2) leads to structure **2**, which is best described as a complex between protonated formaldehyde and ethylene. Ion **2** is characterized by long C···H bonds, with the hydroxyl hydrogen atom of the $[CH_2OH]^+$ fragment bridging the ethylene unit. The C···H bonds (1.946 and 1.977 Å) are significantly longer than those in the nonclassical ethyl cation (1.305 Å at MP2/6-31G(d)) while the $[CH_2OH]^+$ and $C_2H_4$ moieties are only slightly perturbed from their structures as isolated species. Complex **2** is bound with respect to $[CH_2OH]^+$ plus $C_2H_4$ by 73 kJ mol$^{-1}$, and it lies 65 kJ mol$^{-1}$ higher in energy than **1**.

Rotation of the $[CH_2OH]^+$ moiety in **2** leads to structure **3** via **TS:2→3** at 104 kJ mol$^{-1}$. Ion **3** may also be described as an ion−neutral complex between protonated formaldehyde and ethylene, but now the bridge is provided by the carbon atom of $[CH_2OH]^+$ rather than the hydroxyl hydrogen, leading to long bridging C···C bonds. Structure **3** lies 75 kJ mol$^{-1}$ above **1** and 10 kJ mol$^{-1}$ above **2**.

We do not find any evidence for the discrete involvement of the primary 3-hydroxyprop-1-yl cation, $[CH_2CH_2CH_2OH]^+$ (**4′**,

(9) Bowen, R. D.; Williams, D. H.; Hvistendahl, G.; Kalman, J. R. *Org. Mass Spectrom.* **1978**, *13*, 721.
(10) Holmes, J. L.; Rye, R. T. B.; Terlouw, J. K. *Org. Mass. Spectrom.* **1979**, *14*, 606.
(11) McAdoo, D. J.; Hudson, C. E. *Int. J. Mass Spectrom. Ion Processes* **1989**, *88*, 133.
(12) Bouchoux, G.; Penaud-Berruyer, F.; Audier, H. E.; Mourgues, P.; Tortajada, J. *J. Mass Spectrom.* **1997**, *32*, 188.
(13) Nobes, R. H.; Radom, L. *Org. Mass Spectrom.* **1984**, *19*, 385.
(14) Hehre, W. J.; Radom, L.; Schleyer, P. v. R.; Pople, J. A. *Ab Initio Molecular Orbital Theory*; Wiley: New York, 1986.
(15) Frisch, M. J.; Trucks, G. W.; Schlegel, H. B.; Gill, P. M. W.; Johnson, B. G.; Robb, M. A.; Cheeseman, J. R.; Keith, T. A.; Petersson, G. A.; Montgomery, J. A.; Raghavachari, K.; Al-Laham, M. A.; Zakrzewski, V. G.; Ortiz, J. V.; Foresman, J. B.; Cioslowski, J.; Stefanov, B. B.; Nanayakkara, A.; Challacombe, M.; Peng, C. Y.; Ayala, P. Y.; Chen, W.; Wong, M. W.; Andres, J. L.; Replogle, E. S.; Gomperts, R.; Martin, R. L.; Fox, D. J.; Binkley, J. S.; Defrees, D. J.; Baker, J.; Stewart, J. P. P.; Head-Gordon, M.; Gonzalez, C.; Pople, J. A. GAUSSIAN 94, Revision D.1; Gaussian Inc.: Pittsburgh, PA, 1995.
(16) MOLPRO is a package of ab initio programs written by H. J. Werner and P. J. Knowles with contributions from J. Almlof, R. D. Amos, M. J. O. Deegan, S. T. Elbert, C. Hampel, W. Meyer, K. Peterson, R. Pitzer, A. J. Stone, P. R. Taylor, and R. Lindh.
(17) Curtiss, L. A.; Raghavachari, K.; Trucks, G. W.; Pople, J. A. *J. Chem. Phys.* **1991**, *94*, 7221.
(18) Pople, J. A.; Scott, A. P.; Wong, M. W.; Radom, L. *Isr. J. Chem.* **1993**, *33*, 345.
(19) Curtiss, L. A.; Raghavachari, K.; Pople, J. A. *J. Chem. Phys.* **1995**, *103*, 4192.
(20) Nicolaides, A.; Rauk, A.; Glukhovstev, M. N.; Radom, L. *J. Phys. Chem.* **1996**, *100*, 17460.
(21) Scott, A. P.; Radom, L. *J. Phys. Chem.* **1996**, *100*, 16502.
(22) For a discussion of RRKM theory, see: (a) Gilbert, R. G.; Smith S. C. *Theory of Unimolecular and Recombination Reactions*; Blackwell Scientific Publications: Oxford, 1990. (b) Baer, T.; Mayer, P. M. *J. Am. Soc. Mass Spectrom.* **1997**, *8*, 103.
(23) Beyer, T.; Swineheart, D. F. *Commun. ACM* **1973**, *16*, 379.
(24) The entropy of activation ($\Delta S^{\ddagger}$) for the dissociation process should be positive because of the expected loose transition structure. The actual magnitude of $\Delta S^{\ddagger}$ is chosen to be typical of bond cleavage reactions.[22b] The $\Delta S^{\ddagger}$ is not explicitly required, but the frequencies obtained by this fitting procedure are used in the RRKM calculations.

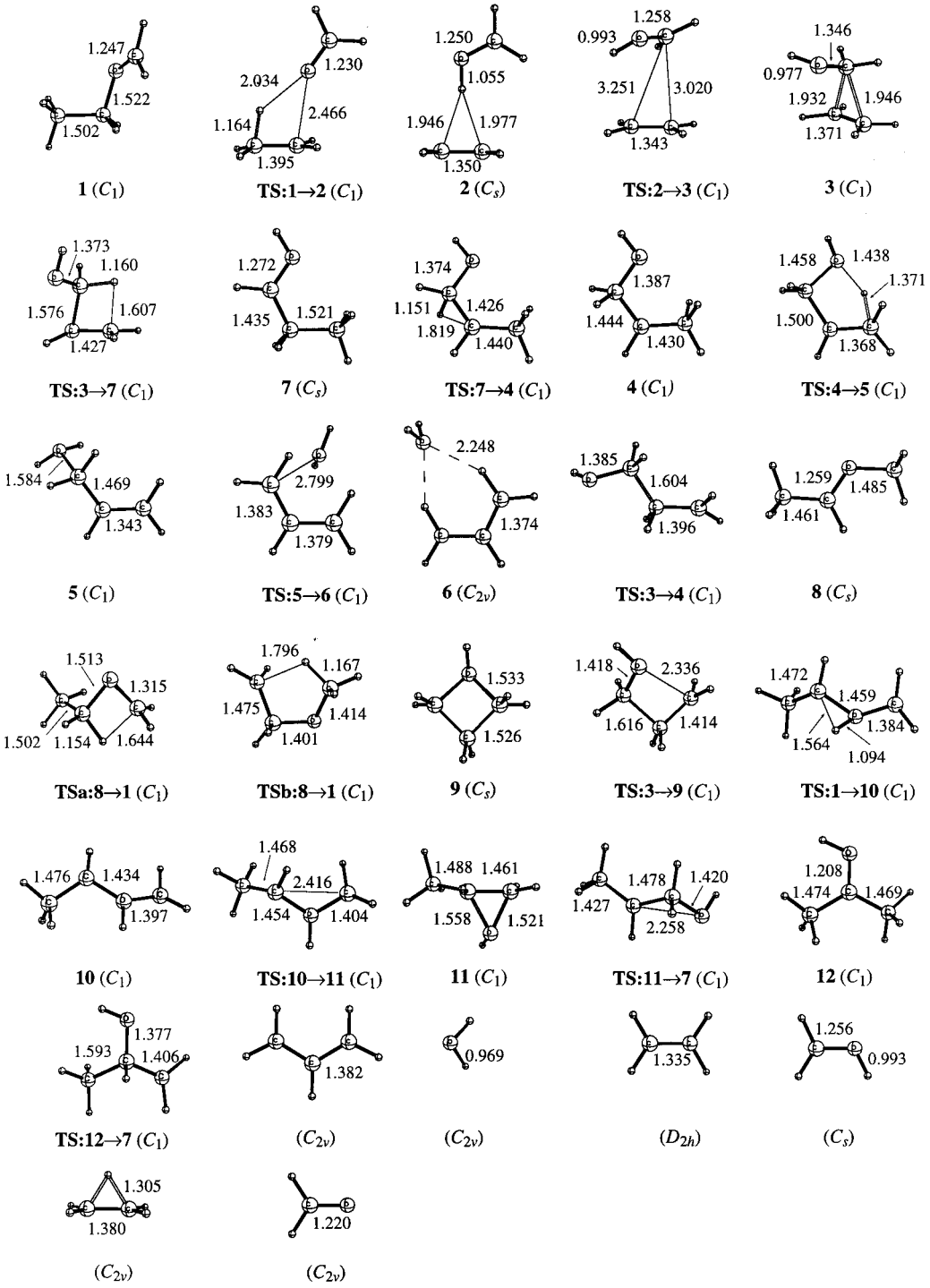


**Figure 1.** Selected MP2/6-31G(d) geometrical parameters. Bond lengths are in angstroms; bond angles are in degrees.

Scheme 1). Instead, the lowest-energy path consists of a concerted ring opening and 1,3-hydrogen shift via **TS:3→7** at 93 kJ mol$^{-1}$, forming protonated propionaldehdye, $[CH_3CH_2CHOH]^+$ (**7**), which lies 55 kJ mol$^{-1}$ below **1**. A 1,2-hydrogen shift in **7** results in the secondary 1-hydroxyprop-2-yl cation, $[CH_3CHCH_2OH]^+$ (**4**), which lies 44 kJ mol$^{-1}$ above **1**. Although **4** is located at a potential minimum on the MP2/6-31G(d) surface (as reflected in all the vibrational frequencies being real), the energy of **TS:7→4** drops below that of **4** at the G2 level (including zero-point vibrational energy). This suggests that **4** at best lies in a very shallow potential well. An alternative direct pathway from **3** to **4** involves concerted ring opening and a 1,2-hydrogen shift. This proceeds via **TS:3→4** at 119 kJ mol$^{-1}$, and thus is energetically less favorable than the pathway via **7**.

A 1,4-hydrogen migration in **4** leads via **TS:4→5** at 112 kJ mol$^{-1}$ to protonated allyl alcohol, $[CH_2{=}CHCH_2OH_2]^+$ (**5**). This structure is characterized by a long C···O bond (1.584 Å). However, the C−C bonds in the allyl moiety of **5** may be distinctly recognized as single (1.469 Å) and double (1.343 Å) so that **5** cannot really be described as a complex between allyl cation and water. Isomer **5** lies just 11 kJ mol$^{-1}$ above **1**.

The $H_2O$ component of **5** can move to a bridging position, as in **6**, via **TS:5→6** at 48 kJ mol$^{-1}$. Complex **6** corresponds to an ion−neutral complex between the allyl cation and water. It is bound with respect to these species by 49 kJ mol$^{-1}$. The

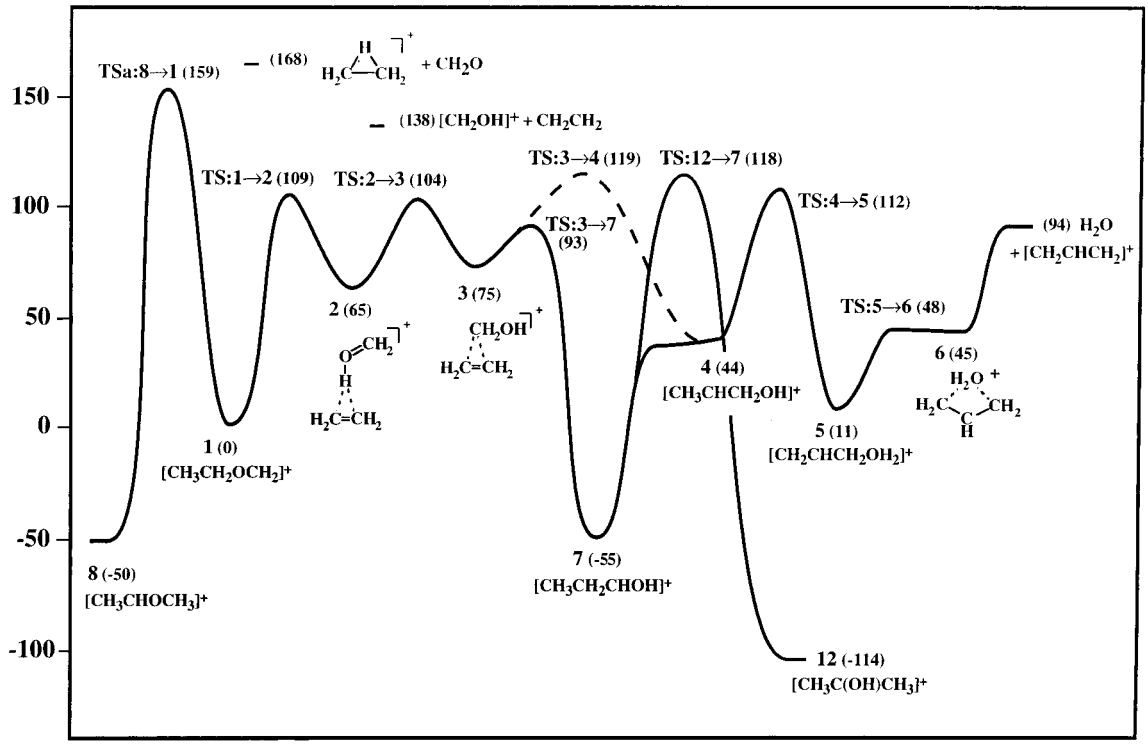


**Figure 2.** Schematic G2 energy profile for water elimination from $CH_3CH_2OCH_2^+$ (**1**). Relative energies (kJ mol$^{-1}$) are given in parentheses.

**Scheme 2**

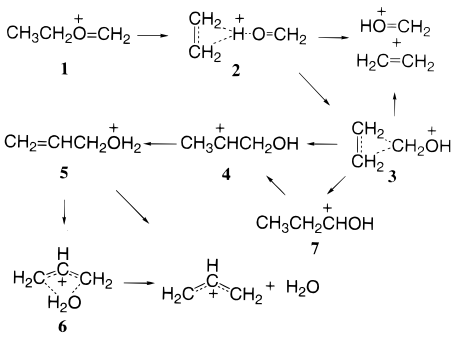

energy of **6** is just 45 kJ mol$^{-1}$ above **1**, but **6** lies in a very shallow potential well, being separated from **5** by a barrier (via **TS:5→6**) of just 3 kJ mol$^{-1}$. Because of the shallowness of the potential well in which it resides, it is not clear whether **6** plays a significant role in the rearrangement/fragmentation of $[CH_3CH_2OCH_2]^+$.

Dissociation from either **5** or **6** leads to the allyl cation plus water at an energy of 94 kJ mol$^{-1}$. This is the lowest-energy pair of dissociation products. The highest-energy point on the reaction path leading from $[CH_3CH_2OCH_2]^+$ (**1**) to these products is **TS:4→5** at 112 kJ mol$^{-1}$, that is, their formation involves a reverse barrier of 18 kJ mol$^{-1}$.

The potential surface of Figure 2 reflects the reaction mechanism displayed in Scheme 2. There are only minor differences between Scheme 2 and the originally postulated mechanism[4] of Scheme 1. The main differences are the noninvolvement as discrete species of **1′** and **4′**, as noted above, and the bridged (rather than open-chain) structure for **3**. The slightly lower-energy pathway made possible by the involvement of **7** in the transformation of **3** to **4** was also not included in Scheme 1. Our potential surface is very similar to that obtained by Bouchoux et al.[12] at the MP2/6-31G(d)//HF/6-31G(d) level. There are no qualitative differences, and even the quantitative agreement is very good, despite a significantly higher level of theory being used in the present study. It is very satisfying that the intricate rearrangements postulated by Bowen and Williams[4] on the basis of a limited amount of experimental data are essentially confirmed by the theoretical calculations.

**Related Mechanisms.** An additional isomer not included in Schemes 1 or 2 but which is very relevant to the rearrangement and dissociation pathways, as discussed below, is $[CH_3CHOCH_3]^+$ (**8**). This is found to lie 50 kJ mol$^{-1}$ below **1**. Two possible isomerization pathways from **8** to **1** have been postulated,[7a] namely a direct 1,3-hydrogen shift or a two-step process involving a 1,2-hydrogen shift to give $[CH_2CH_2OCH_3]^+$ followed by a 1,4-hydrogen shift. We find that the 1,3-hydrogen shift occurs via **TSa:8→1** at 159 kJ mol$^{-1}$ (relative to **1**), corresponding to a barrier for **8→1** of 209 kJ mol$^{-1}$. Our calculations indicate that in the second pathway the 1,2- and 1,4-hydrogen shifts can occur in a concerted manner via **TSb: 8→1** at a considerably higher energy, corresponding to a barrier of 275 kJ mol$^{-1}$. There is no involvement of $[CH_2CH_2OCH_3]^+$ as a discrete intermediate (minimum energy structure), but **TSb: 8→1** does resemble such a structure.

Another $[C_3H_7O]^+$ isomer not included in Schemes 1 or 2 is protonated oxetane (**9**). It is characterized by quite long C−O bonds (1.533 Å) and lies 20 kJ mol$^{-1}$ above **1**. It is of relevance to labeling experiments since it could allow exchange of hydrogen and carbon labels in **3** via the transition structure **TS: 3→9** at 118 kJ mol$^{-1}$. This is also discussed below.

It has been suggested[10] that it may be possible for **1** to isomerize to **4** via protonated methyloxirane (**11**) in a pathway involving no ion−neutral complexes. The pathway that we have characterized for this transformation begins with a 1,2-hydrogen shift via **TS:1→10** with a barrier of 396 kJ mol$^{-1}$, to form the high-energy species $[CH_3CHOHCH_2]^+$ (**10**) at 332 kJ mol$^{-1}$, followed by ring closure to give protonated methyloxirane (**11**). Although **10** is a true minimum on the MP2/6-31G(d) potential energy surface, the energy of **TS:10→11** drops below that of **10** at the G2 level (including ZPE), indicating little or no barrier for the **10→11** cyclization. Thus **TS:1→10** is effectively the

**Table 1.** Theoretical and Experimental Heats of Formation ($\Delta_f H_{298}$)

| species | | G2 | experiment[a] |
|---|---|---|---|
| $[CH_3CH_2OCH_2]^+$ | (**1**) | 612 | 593 |
| $[CH_2CH_2\ HOCH_2]^+$ | (**2**) | 678 | |
| $[CH_2CH_2\ CH_2OH]^+$ | (**3**) | 684 | |
| $[CH_3CHCH_2OH]^+$ | (**4**) | 654 | (673)[b] |
| $[CH_2CHCH_2OH_2]^+$ | (**5**) | 620 | (602)[b] |
| $[CH_2CHCH_2\ OH_2]^+$ | (**6**) | 659 | |
| $[CH_3CH_2CHOH]^+$ | (**7**) | 554 | 550 |
| $[CH_3CHOCH_3]^+$ | (**8**) | 561 | 562 |
| $[CH_2CH_2CH_2OH]^+$ | (**9**) | 626 | 625 |
| $[CH_3CHOHCH_2]^+$ | (**10**) | 942 | |
| $[CH_3CHCH_2OH]^+$ | (**11**) | 633 | 620 |
| $[CH_3C(OH)CH_3]^+$ | (**12**) | 495 | 490 |
| $H_2O + [CH_2CHCH_2]^+$ | | 709 | 709 |
| $CH_2CH_2 + [CH_2OH]^+$ | | 752 | 755 |
| $CH_2O + [CH_3CH_2]^+$ | | 784 | 793 |

[a] All experimental values are taken from ref 25 unless otherwise noted. [b] Estimated in ref 9.

transition structure for the transformation from **1** to **11**. Protonated methyloxirane (**11**) lies 26 kJ mol$^{-1}$ above **1**. A ring opening via **TS:11→7** at 83 kJ mol$^{-1}$ yields **7**, which can isomerize to **4** and then continue as described above. However, due to the very high energy of **10**, this mechanism is not competitive with that of Scheme 2 involving ion−neutral complexes.

Finally, it has been suggested that it is possible for protonated acetone, $[CH_3C(OH)CH_3]^+$ (**12**), to rearrange to **7**. We find that protonated acetone, which lies 114 kJ mol$^{-1}$ below **1**, can isomerize directly to **7** via **TS:12→7** at 118 kJ mol$^{-1}$. We find no evidence for the existence of $[CH_3CH(OH)CH_2]^+$, which was proposed as an intermediate for this isomerization,[7b] although **TS:12→7** bears a strong resemblance to such a structure. The consequences of forming **7** from **12** are discussed below.

**Comparisons with Experimental Thermochemical Data.** Calculated heats of formation at 298 K ($\Delta_f H_{298}$) are compared with available experimental data[9,25] in Table 1. The agreement between theory and experiment is generally within the G2 target accuracy of ±10 kJ mol$^{-1}$. Two species for which directly measured experimental values are available that show somewhat larger discrepancies are **1** and **11**, the differences being 19 and 13 kJ mol$^{-1}$, respectively. The heats of formation for **4** and **5** are only estimated quantities,[9] and these differ by larger amounts from the G2 values.

The calculated barriers for the formation of the various fragmentation products may be compared with values determined from measured appearance energies. The calculated values for the barriers for the formation of $H_2O$ and $C_2H_4$ are 112 and 138 kJ mol$^{-1}$, which are somewhat higher than the reported experimental values[7a] of 96 ± 13 and 117 ± 13 kJ mol$^{-1}$, respectively. We note, however, that obtaining the experimental values requires the use of heats of formation of the precursor neutral and the relevant parent ion, so the results would be changed by employing updated values for these quantities.

The experimental appearance energies for the elimination of $H_2O$ and $C_2H_4$ from **8** are each found to be 249 ± 13 kJ mol$^{-1}$.[7a] The coincidence of these values is consistent with the fact that the energy barriers for both of these processes are determined by the energy of **TSa:8→1** (Figure 2). Quantitatively, the experimental barrier (249 kJ mol$^{-1}$) is somewhat higher than the calculated value of 209 kJ mol$^{-1}$, as found also in other recent theoretical work.[27]

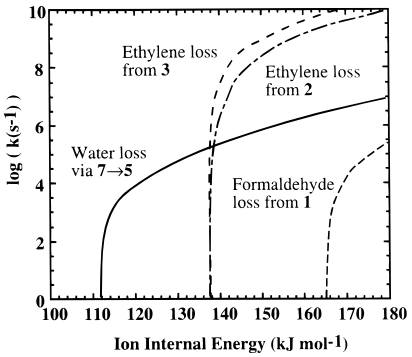


**Figure 3.** RRKM rate constants (log *k*) calculated as a function of internal energy (*E*) for ethylene loss from **2** and **3**, formaldehyde loss from **1**, and the rate-determining step (**7→5**) for water loss. Energy is measured relative to that of **1**.

Experimental appearance energies for the elimination of $H_2O$ and $C_2H_4$ from **12** are found to coincide at a value of 268 ± 20 kJ mol$^{-1}$,[7b] again consistent with the fact that both are determined by the energy of **TS:12→7**. The experimental barrier is again somewhat higher than the calculated value of 232 kJ mol$^{-1}$.

**Relationship to Observed Rearrangement/Fragmentation Behavior.** The calculated potential energy profile (Figure 2) and the results of RRKM calculations of rate constants for the loss of ethylene from the ion−neutral complexes **2** and **3** and for the rate-determining step (**7→5**) for loss of water from $[CH_3CH_2OCH_2]^+$ (**1**) (Figure 3) can be used to rationalize a number of experimental observations. First, it is clear from Figure 2 that the lowest-energy fragmentation process for **1** corresponds to the loss of a water molecule, requiring 112 kJ mol$^{-1}$. This is consistent with the observation that water elimination is the dominant reaction of the metastable ion **1**.[5,6,9] In addition, the results of Figure 3 show that, within the metastable time frame ($k \approx 10^4-10^6$ s$^{-1}$), water loss should take place over a much wider energy range than ethylene loss, again consistent with the dominance of water elimination. Figure 3 also shows that as the time frame is changed to encompass larger values of *k*, water loss becomes slow relative to ethylene loss. This is reflected in the ratio of water loss to ethylene loss increasing significantly in going from the first field-free region to the second field-free region of the mass spectrometer.[7a]

The rate constant curves in Figure 3 are characteristic of a situation in which there is a lower-energy rearrangement process (water loss) and a higher-energy direct dissociation (ethylene loss). Under these circumstances, the rearrangement process is favored by low-energy ions and the direct dissociation is favored by high-energy ions. It is therefore not surprising that, in contrast to the dominant water loss in the metastable ion spectrum of **1**, the collision-induced dissociation spectrum is dominated by ethylene loss and also shows some formaldehyde loss,[6c,7a] even though these last two processes require 26 and 56 kJ mol$^{-1}$, respectively, more energy than water loss.

The decomposition of the metastable $[CH_3CHOCH_3]^+$ ion (**8**) results in elimination of ethylene, formaldehyde, and small amounts of water,[5,6b,7a] all of which may be lost after rearrangement to $[CH_3CH_2OCH_2]^+$ (**1**). It has been observed that the metastable spectrum of **8** shows some similarity to the collision-

(25) Lias, S. G.; Bartmess, J. E.; Liebman, J. F.; Holmes, J. L.; Levin, R. D.; Mallard, W. G. *J. Phys. Chem. Ref. Data Suppl.* **1988**, *17*.

(26) Tortajada, J.; Audier, H. E.; Monteiro, C.; Mourgues, P. *Org. Mass Spectrom.* **1991**, *26*, 913.

(27) Hudson, C. E.; McAdoo, D. J. *J. Am. Soc. Mass Spectrom.* **1998**, *9*, 130.

induced dissociation mass spectrum of **1**.[6c,7a] This result can be readily rationalized by noting that the existence of a substantial barrier (209 kJ mol$^{-1}$) for isomerization of **8** to **1** will result in the formation of **1** with considerable excess energy. The energy of **TS:8→1** is above that required for ethylene elimination and is only marginally (9 kJ mol$^{-1}$) below that required for formaldehyde elimination. In fact, due to the large barrier, it would be expected that the isomerization of **8** to **1** would not occur on the metastable time frame until energies significantly above threshold have been reached. Thus, RRKM calculations indicate that metastable isomerization will not begin until about 35 kJ mol$^{-1}$ above the threshold, well in excess of the energy needed to eliminate formaldehyde. Hence, our calculated barrier is consistent with significant loss of formaldehyde from **8**.

Metastable protonated acetone, $[CH_3C(OH)CH_3]^+$ (**12**), also loses water and ethylene.[6,7b] However, the abundances are different from those observed for ion **1**, with ethylene elimination being slightly favored over water elimination.[6,7b] This is again readily explained by the fact that ions that have isomerized from **12** to **7** will have surmounted a large barrier (118 kJ mol$^{-1}$ relative to **1**) and hence have a significant amount of internal energy. As noted above for the isomerization of **1** to **8**, the ions will actually have significantly more energy than this barrier suggests, with RRKM calculations indicating that metastable isomerization of **7** to **12** will not occur until an energy of about 165 kJ mol$^{-1}$ above **1** is reached. Because higher internal energies favor ethylene elimination, metastable **12** thus shows a greater proportion of ethylene elimination than does **1**. It should also be noted that metastable **12** has sufficient energy to eliminate formaldehyde. However, formaldehyde elimination is generally slow relative to ethylene and water elimination (Figure 3) and is therefore not observed in metastable ion decompositions. At the higher internal energies represented in the first field-free region, formaldehyde elimination becomes more competitive and a small extent of formaldehyde elimination is observed.[6b]

**Label Exchange Mechanisms and Kinetic Analysis.** Extensive labeling studies have been reported for various deuterated analogues of **1**.[9−12] It has been found that exchange of the hydrogen atoms within the ethyl group of **1** (henceforth referred to as ethyl hydrogens) and exchange of the ethyl hydrogens with those in the $OCH_2$ group (referred to as methylene hydrogens) occur at different rates,[12] suggesting differing mechanisms for the two processes. Exchange of the ethyl hydrogens is straightforward and can be attributed to reversible isomerization of **1** and **2**. Methylene exchange can be caused either by reversible isomerization between **3** and **7** or between **3** and **9**. The intervention of **7** or **9** can be distinguished by noting that the latter would have the added effect of causing loss of identity of $^{13}$C-labels. Early experiments by Bowen et al. indicated that significant amounts of $^{13}$C-label exchange occurs during ethylene elimination from labeled analogues of **1**[9] and **7**.[8b] However, later labeling experiments on **1**[11] and **7**[10] and ICR experiments on mixtures of $[^{13}CH_2OH]^+$ and $CH_2$-$CH_2$ have failed to observe significant $^{13}$C-label exchange.[12,26]

Our RRKM calculations of reaction rates assist in the understanding of the label-exchange processes. A plot of the log of the calculated rate constants versus internal energy for the possible isomerization processes of ion **3** is shown in Figure 4. It can be seen that at energies appropriate to metastable ethylene elimination (∼138 kJ mol$^{-1}$), the rate constant for isomerization of **3** to **9** is roughly an order of magnitude slower than isomerization to **7** and approximately 3 orders of magnitude slower than isomerization back to **2**. The isomerization of **3** to **4** is found to be comparably slow. Our calculations thus support the conclusion that isomerization of **3** to **9** does not occur to any great extent and hence only small amounts of $^{13}$C-label exchange should take place. Label exchange between the methylene hydrogens and the ethyl hydrogens is predicted to be predominantly caused by the reversible isomerization of **3** and **7**.

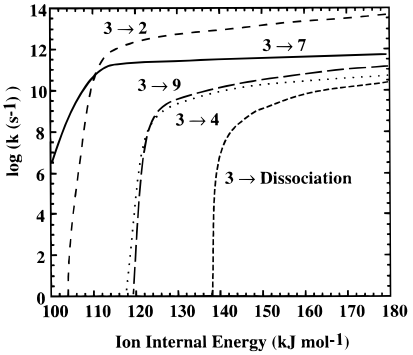


**Figure 4.** RRKM rate constants (log $k$) calculated as a function of internal energy ($E$) for the isomerization processes of **3**. Energy is measured relative to that of **1**.

The labeling experiments show that during water elimination there is a pronounced tendency for $\beta$-hydrogen transfer to oxygen to occur, whereas during ethylene elimination the labels are distributed almost statistically among all the available sites.[9,11,12] Interesting labeling behavior, which will be discussed later, is also observed for **7** and **12**. To address these issues, we have carried out an analysis of the reaction kinetics. Assuming as before that ethylene elimination occurs only from **2** and **3** and that the rate-limiting step to water elimination from **1** is isomerization of **7** to **5** (via **TS:4→5**), which is consistent with recent experiments,[12] we can write the rate equations for the processes involved in label exchange as follows:

$$\frac{d[\mathbf{1}]}{dt} = -k_{12}[\mathbf{1}] + k_{21}[\mathbf{2}] \quad (2)$$

$$\frac{d[\mathbf{2}]}{dt} = -(k_{21} + k_{23} + k_{2d})[\mathbf{2}] + k_{12}[\mathbf{1}] + k_{32}[\mathbf{3}] \quad (3)$$

$$\frac{d[\mathbf{3}]}{dt} = -(k_{32} + k_{37} + k_{3d})[\mathbf{3}] + k_{23}[\mathbf{2}] + k_{73}[\mathbf{7}] \quad (4)$$

$$\frac{d[\mathbf{7}]}{dt} = -(k_{73} + k_{7d})[\mathbf{7}] + k_{37}[\mathbf{3}] + k_{12-7}[\mathbf{12}] \quad (5)$$

$$\frac{d[\mathbf{12}]}{dt} = -k_{12-7}[\mathbf{12}] \quad (6)$$

$$\frac{d[H_2O]}{dt} = k_{7d}[\mathbf{7}] \quad (7)$$

$$\frac{d[C_2H_4]}{dt} = k_{2d}[\mathbf{2}] + k_{3d}[\mathbf{3}] \quad (8)$$

where $k_{xy}$ is the rate constant for isomerization of ***x*** to ***y*** and $k_{xd}$ is the rate of dissociation of ***x***. It is possible to solve these equations and hence obtain the abundances of all species involved at any specified time. However, this does not tell us anything about the behavior of labeled species.

To examine the isotope distribution patterns, we have therefore extended the system of rate equations to describe the behavior of all the possible singly deuterated analogues of **1**,

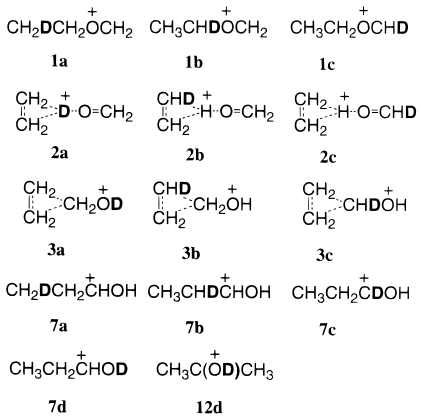


**Figure 5.** Singly deuterated analogues of ions **1**, **2**, **3**, **7**, and **12**.

**Table 2.** Calculated and Experimental Isotope Distributions for Water Elimination[a]

| | $H_2O$ | | | | HOD | | | |
|---|---|---|---|---|---|---|---|---|
| species | $E =$ 120 | $E =$ 128 | $E =$ 170 | expt[b] | $E =$ 120 | $E =$ 128 | $E =$ 170 | expt[b] |
| **1a** | 65 | 69 | | | 34 | 31 | | |
| **1b** | 74 | 71 | | | 26 | 29 | | |
| **1c** | 78 | 75 | | | 22 | 25 | | |
| **7c** | 83 | 77 | | 88 | 17 | 23 | | 12 |
| **7d** | 32 | 60 | | 31 | 68 | 40 | | 69 |
| **12d** | | | 9 | 10[c] | | | 91 | 90[c] |
| statistical | 71 | 71 | 71 | 71 | 29 | 29 | 29 | 29 |

[a] Calculated values obtained using rate constants derived for ions **1** with internal energy $E$ (kJ mol$^{-1}$). Isotopomers are displayed in Figure 5. [b] Average of experimental values from refs 9, 11, and 12 unless otherwise noted. [c] From ref 6c.

**2**, **3**, and **7** and the O-deuterated analogue of **12** (see Figure 5 and eqs S1−S18 of the Supporting Information). We have made the additional assumption that there are no isotope effects. Equations S1−S18 have been solved numerically and the results used to make quantitative predictions of the abundances for the eliminated species from the metastable singly deuterated ions. Since the decomposition of metastable ions occurs in a fairly narrow time window ($10^{-6}$−$10^{-5}$ s), we are interested in the change in abundance that occurs during this time interval. We must also choose an appropriate energy at which to calculate the unimolecular rate constants. Because the rate-limiting steps for ethylene elimination, namely dissociation of either complex **2** or complex **3**, have no reverse barrier, the metastable elimination of ethylene will occur near threshold. Hence, for ethylene we have calculated the rates for an internal energy just above the thermochemical threshold (138.1 kJ mol$^{-1}$). For water elimination, however, the choice is not so obvious. Our RRKM calculations indicate that metastable water elimination can occur over a range of internal energies of **1**, ranging from approximately 120 to 138 kJ mol$^{-1}$, at which stage ethylene elimination becomes more favorable (see Figure 3). It is likely that significant changes in the isotope distribution will occur over this energy range, so the rate constants have been calculated at two internal energies, 120 and 128 kJ mol$^{-1}$. Isotope distributions for both water and ethylene elimination have also been calculated at 170 kJ mol$^{-1}$, just above the onset calculated for metastable isomerization (see above), to examine label exchange in the dissociation of metastable **12**.

Calculated isotope distributions for water elimination from the deuterated analogues of **1** and for **7c**, **7d**, and **12d** (see Figure 5) are compared with available experimental data in Table 2. Statistical results are also shown for comparison. It can be seen that, at an energy of 120 kJ mol$^{-1}$, **1a** displays a greater than statistical loss of HOD while **1b** and **1c** show less than statistical loss, consistent with $\beta$-transfer to oxygen being favored, as experimentally observed.[9,11,12] When the energy is increased to 128 kJ mol$^{-1}$, the abundances approach their statistical value but still display a slight tendency for $\beta$-transfer. At 120 kJ mol$^{-1}$, **7d** shows a much greater than statistical loss of HOD while **7c** shows a greater than statistical loss of $H_2O$, consistent with a tendency for retention of the oxygen-bound hydrogen during water elimination, as is observed experimentally.[9,11,12] The calculated abundance of HOD elimination from **7c** (17%) is the same as that which would result from retention of the oxygen-bound hydrogen along with random selection of the second water hydrogen from the six other hydrogens, that is, significant exchange of the carbon-bound hydrogens occurs, again in agreement with experiment.[9,11,12] At the higher energy of 128 kJ mol$^{-1}$ the abundances for water elimination from **7c** and **7d** also approach the statistical result but the trends observed at lower energies still remain to a lesser extent. At the energies appropriate to water elimination from **12** (170 kJ mol$^{-1}$), there is a very pronounced tendency for retention of deuterium on oxygen, that is, dominant loss of partially deuterated water is observed. At these high energies, isomerization of **7** to **5**, which leads to water loss, is of comparable rate to isomerization of **7** to **3**. Hence, dissociation occurs before significant label exchange can occur, and the label remains predominantly attached to oxygen. In the cases where experimental labeling data for water loss from **1** and **7** exist, good agreement between theory and experiment is seen at the lower internal energy. Good agreement with experimental labeling results is also observed for **12d**. The calculated distributions for elimination from **12** of 29% $H_2O$ and 71% ethylene are also in satisfactory agreement with the experimental results, ranging from 31 to 46% $H_2O$ and 69 to 54% $CH_2CH_2$.[6,7b]

**Table 3.** Calculated and Experimental Isotope Distributions for Ethylene Elimination[a]

| | $CH_2CH_2$ | | | $CHDCH_2$ | | |
|---|---|---|---|---|---|---|
| species | $E =$ 138.1 | $E =$ 170 | expt[b] | $E =$ 138.1 | $E =$ 170 | expt[b] |
| **1a** | 43 | | | 57 | | |
| **1b** | 43 | | | 57 | | |
| **1c** | 43 | | | 57 | | |
| **7c** | 43 | | 42 | 57 | | 58 |
| **7d** | 43 | | 66 | 57 | | 34 |
| **12d** | | 38 | 66[c] | | 62 | 34[c] |
| statistical | 43 | 43 | 43 | 57 | 57 | 57 |

[a] Calculated values obtained using rate constants derived for ions **1** with internal energy $E$ (kJ mol$^{-1}$). Isotopomers are displayed in Figure 5. [b] Average of experimental values from refs 9, 11, and 12 unless otherwise noted. [c] From ref 6c.

For ethylene elimination, our calculations (Table 3) predict a statistical distribution of labels for all species shown, which is consistent with experiment for all but two related cases. In contrast to the predicted statistical behavior, **7d** is found experimentally to show a much greater than statistical loss of $CH_2CH_2$. A possible explanation for this behavior is that some other pathway is in operation that allows ion **7** to eliminate ethylene with retention of the deuterium label on oxygen. This is supported by experiments[10] which suggest an additional pathway for ethylene elimination for **7d** ions, with the measured kinetic energy release for ions where label exchange has occurred being different from that of ions that retain the label. These experiments also show that the kinetic energy release of those ions that exhibit label exchange is the same as that for ethylene elimination from ion **1**.[10] This suggests that label exchange in ion **7d** occurs via a common intermediate to **1** (i.e.,

via **2** or **3**), while a separate mechanism applies for eliminations of ethylene where the label is retained on oxygen. It has previously been suggested[9] that a competing mechanism for ethylene elimination from **7** is sequential 1,2-hydrogen shifts from **7** to form $[CH_3CHCH_2OH]^+$ (**4**) and then $[CH_2CH_2CH_2OH]^+$ (**4′**), with the latter dissociating by a simple bond cleavage resulting in loss of (label-retaining) ethylene. This mechanism would result in an increase in label-retaining eliminations for **7d** and would also account for the different kinetic energy release value for ethylene eliminated with the label retained on oxygen. A similar argument can account for the difference between our calculated results and experiment for **12d**. Thus, since **12d** initially isomerizes to **7d**, the above mechanism would also be consistent with the observed preference for label-retaining eliminations.

## Concluding Remarks

The decomposition of $[CH_3CH_2OCH_2]^+$ proceeds via a mechanism in which the involvement of ion−neutral complexes as intermediates plays a crucial role. Mutual reorientation of the two components of the ion−neutral complex **2** to form **3** allows a rearrangement that would be considerably more difficult via conventionally bonded species. Our proposed mechanism (Scheme 2) is very similar to that originally proposed by Bowen and Williams (Scheme 1) and strongly supports the results of recent calculations carried out at a somewhat lower level of theory. The reaction profile, along with an RRKM study of the reaction kinetics, shows that Scheme 2 can account for the results of extensive deuterium- and $^{13}C$-labeling experiments. There is generally good agreement with available experimental thermochemical data.

**Acknowledgment.** We gratefully acknowledge generous allocations of time on the Fujitsu VPP300 and SGI Power Challenge computers of the Australian National University Supercomputing Facility. We also thank Dr. Paul Mayer and Dr. Michael Collins for many helpful discussions and for comments on the manuscript.

**Supporting Information Available:** Total G2 energies (Table S1), GAUSSIAN 94 archive entries of the MP2/6-31G-(d) optimized geometries (Table S2), and rate equations for the kinetic scheme (eqs S1−S18) (11 pages, print/PDF). See any current masthead page for ordering information and Web access instructions.

JA9741786